

Article

Effect of Time and Voltage on the Electrophoresis Deposition of Zinc Oxide Thin Films for Photovoltaic Applications

Vanja Fontenele Nunes ¹, Manuel Pedro Fernandes Graça ^{2,*}, Imen Hammami ², Ana Fabíola Leite Almeida ³
and Francisco Nivaldo Aguiar Freire ^{1,3}

¹ Department of Science and Engineering Materials, Federal University of Ceará, Fortaleza 60440-554, Ceará, Brazil; vanjafontenele@gmail.com (V.F.N.); nivaldo@ufc.br (F.N.A.F.)

² I3N and Physics Department, Aveiro University, 3810-193 Aveiro, Portugal; imenhammami@ua.pt

³ Department of Mechanical Engineering, Federal University of Ceará, Fortaleza 60455-760, Ceará, Brazil; anafabiola@ufc.br

* Correspondence: mpfg@ua.pt

Abstract: Electrophoretic deposition is a straightforward, environmentally friendly, and cost-effective technique for depositing and synthesizing nanomaterials, particularly nanofilms of semiconductors. Key parameters in electrophoresis include deposition time and voltage. Zinc oxide, a semiconductor of significant interest in solar energy research, possesses favorable characteristics, notably, a band gap value of approximately 3.33 eV. In the realm of dye-sensitized solar cells, which represent the third generation of solar cells, zinc oxide has emerged as a compelling choice for a photoanode. This study focused on depositing thin films of zinc oxide through electrophoresis and applying them as photoanodes in dye solar cells. The results demonstrated that the electrodeposited films exhibited good reflectance in the visible spectrum (~60–90%), a band gap energy of 3.28 eV, and an incident photon conversion efficiency of approximately 4.48% for the electrodeposited film at 80 V for 5 min.

Keywords: electrophoretic deposition; thin films; zinc oxide; deposition time



Citation: Nunes, V.F.; Graça, M.P.F.; Hammami, I.; Almeida, A.F.L.; Freire, F.N.A. Effect of Time and Voltage on the Electrophoresis Deposition of Zinc Oxide Thin Films for Photovoltaic Applications. *Appl. Sci.* **2024**, *14*, 1202. <https://doi.org/10.3390/app14031202>

Academic Editor:
Alejandro Pérez-Rodríguez

Received: 15 December 2023
Revised: 26 January 2024
Accepted: 29 January 2024
Published: 31 January 2024



Copyright: © 2024 by the authors. Licensee MDPI, Basel, Switzerland. This article is an open access article distributed under the terms and conditions of the Creative Commons Attribution (CC BY) license (<https://creativecommons.org/licenses/by/4.0/>).

1. Introduction

In the relentless pursuit of clean and efficient energy sources, solar energy has emerged as a focal point of considerable interest. At the forefront of solar energy production, photovoltaics stands as a pivotal avenue, evolving through distinct generations to enhance their capabilities.

The first generation, characterized by crystalline silicon, laid the foundation for solar technology. Building upon this, the second generation introduced amorphous silicon, refining the efficiency and expanding the potential applications of solar cells. The third generation represents a leap forward, incorporating innovative technologies such as nanocrystalline materials, quantum dots, organic compounds, and dye-sensitized solar cells, diversifying the landscape of solar energy capture. Advancing even further, the fourth generation, featuring materials like graphene, exemplifies the cutting edge of solar technology. Graphene, with its exceptional electrical conductivity and flexibility, holds promise for revolutionizing solar cells, paving the way for unprecedented efficiency and versatility in energy production [1,2].

This dynamic progression across generations underscores the ongoing commitment to harnessing the full potential of solar energy, driving us towards a cleaner and more sustainable energy future [1]. Dye-sensitized solar cells (DSSC) belong to the third generation, comprising an electrode, a counter electrode, an electrolyte, and a dye. In this system, light excites an electron from the dye, initiating a journey through the electrode and the external circuit, ultimately being captured by the counter electrode, thereby regenerating the electrolyte as 3I⁻/I⁻3. Electrolyte 3I⁻/I⁻3 is the electrolyte used, with a specific ratio of three iodine molecules (I₃) to one iodide ion (I⁻) in the redox process. In this process, the iodide

regenerates with the electron that goes through the counter electrode in the DSSC. It is important that there is no recombination between the dye/electrolyte to improve efficiency.

Dye-sensitized solar cells (DSSCs) differ from other types of solar cells due to their unique design involving three essential processes, light absorption leading to the generation of electric charges, electron transport, and hole transport, all occurring through three distinct materials. This distinctive structure classifies them as highly interfacial devices. To maximize the energy conversion efficiency of DSSCs, it is crucial to improve both the charge transfer and transport rates. This enhancement ensures that a significant proportion of electrons can be extracted for external loads, minimizing the likelihood of electron–hole pair recombination. Notably, given the interdependence of transport and transfer rates, simultaneous optimization of electron transfer rates is imperative for achieving higher-efficiency DSSCs [3,4]. Commonly, the electrode is composed of oxides such as TiO_2 , SnO_2 , ZnO , etc. [5]. Zinc oxide (ZnO) stands out as a promising material for DSSC electrodes due to its high electron mobility, wide bandgap of around 3.33 eV (similar to TiO_2), and transparency in the visible light range, allowing light to penetrate and reach the dye molecules within the DSSC and, hence, facilitate effective light absorption and subsequent generation of electron–hole pairs [6–8]. The chemical stability of ZnO is critical, as it prevents DSSCs from degrading over time, even when exposed to environmental factors, thereby ensuring their durability and continued functionality [9]. Moreover, the flexibility in the synthesis of ZnO and the control over its morphology are additional factors that contribute to its suitability for DSSC applications. It has been reported that the nanoporous dye-sensitized ZnO films exhibit a remarkable propensity for ultrafast electron injection from the dye to the conduction band of the ZnO particles [10,11]. The diverse array of ZnO growth morphologies, including nanocombs, nanohelices, nanorings, nanosprings, nanowires, nanobelts, and nanocages, renders ZnO a highly functional material [12–14]. ZnO has emerged as a promising material not only for DSSCs but also for various other applications, including photocatalytic processes [15]. In photocatalysis, ZnO efficiently utilizes visible light to degrade organic pollutants and mineralize them in water [15,16]. Additionally, ZnO exhibited the potential to be used in processes like carbon monoxide oxidation, methanol steam reforming, and hydrogen evolution [17].

Various methods are employed for synthesizing thin films of zinc oxide, including co-precipitation [15,18], electrophoresis [19], ultrasonic techniques [20], and spray deposition [21]. Electrophoretic deposition (EPD) has emerged as a low-cost and efficient method that operates at room temperature. In an EPD electrochemical cell, deposition occurs as charged solution particles of the electrolyte flow toward an electrode with an opposite charge (positive or negative). This flow is induced by an external voltage source, allowing for easy adjustment of parameters such as voltage and deposition time [22]. It is a method widely used for thin films; Lyalin. E. et al. [23] deposited thin film membranes of tetragonal $\text{Li}_7\text{La}_3\text{Zr}_2\text{O}_{12}$ for use in batteries. Nunes. V.F et al. [19], electrodeposited zinc oxide at 30, 40, and 50 V for application on DSSCs; Proller. S. et al. [24], deposited organic thin films by EPD, achieving a power conversion efficiency of 25%. Das. D. et al. [25] fabricated nanostructured zirconia thin films with the EPD methodology, obtaining a current density of 1.08 A/cm^2 . Liu. Y et al. [26], developed a simple EPD method for MoSe_2 nanosheets/carbon cloth electrodes. Zargazi, M. and Entezari M. H. [27] completed anodic electrophoretic deposition of Bi_2WO_6 thin films with high photocatalytic activity and a film thickness of 627 nm. Pikalova. E et al. [28] used electrophoretic deposition to fabricate thin film membranes of BaCeO_3 and CeO_2 for anode-supported solid oxide fuel cells. Hassam. C. L. et al. [29] electrodeposited transparent thin films of Sb_2S_3 . For solar cells, Shakir. S et al. [30] electrodeposited TiO_2 on DSSCs. Yaacob. K.A [31] performed EPD using CdSe-TiO_2 nanocomposites for quantum dot solar cells; Vasanth. A [32] also used EPD for graphene oxide on DSSCs. The use of EPD with ZnO has not been widely explored. This method has been primarily applied with other materials, as mentioned above. Consequently, the authors employed a simple EPD method with ZnO for DSSCs, a combination that has not been extensively reported in the literature in recent years. Aghili

et al. [33] utilized electrophoretically coated zinc oxide for biomedical purposes at low voltages. In this work, we investigated the use of high voltages, ranging between 60 and 80 V, a practice not commonly reported in the literature. The applied voltage, along with the deposition time, significantly influences the coating's thickness and band gap. These factors are essential for the application of photovoltaic devices.

This study involved the deposition of thin zinc oxide films, varying both voltage and deposition time to evaluate their impact on the optical properties of the oxide. Subsequently, these films were utilized as electrodes in dye-sensitized solar cells to investigate how changes in voltage and deposition time could influence the photovoltaic performance of the cell. This work aims to contribute to a more comprehensive understanding of the electrophoretic deposition of ZnO, particularly when applied to DSSCs. This involves analyzing and comparing the voltage and time parameters specifically for zinc oxide.

2. Materials and Methods

2.1. Synthesis of the Films

The zinc oxide (ZnO) powder, with a high purity of 99% and a molecular weight of 81.37 g/mol (PA), was procured from Vetec. Magnesium nitrate ($\text{Mg}(\text{NO}_3)_2 \cdot 6\text{H}_2\text{O}$), which created charged particles in the solution for the applied potential difference (ddp), was acquired from Dinâmica-Química Contemporânea Lda, Brazil. These were mixed in an ethanol (Synth) suspension at concentrations of 8 g/L and 0.1 g/L, respectively [19]. The fluorine-doped tin oxide (FTO), N179 dye, FTO with platinum, and the electrolyte Iodolyte AN-50 were acquired from Solaronix©, Aubonne, Switzerland. N719 is a dye with the chemical formula $\text{C}_{58}\text{H}_{86}\text{N}_8\text{O}_8\text{RuS}_2$, also known as Ruthenizer 535-bisTBA, belonging to the ruthenium dye family and used in the wavelength range up to 750 nm. AN-50 is a redox couple with the iodide/tri-iodide formula, regenerated by the electron that passes through the counter electrode in the cell, with a concentration of 50 mM.

Electrophoretic deposition was carried out using a voltage source k33-300V, Kasvi.

The electrophoresis deposition followed the following steps:

1. The electrophoretic deposition took place in a simple two-electrode cell, with FTO serving as the anode and platinum as the cathode. The volume of the ZnO suspension in ethanol was 50 mL. Deposition occurred at applied voltages of 60 V, 70 V, and 80 V, with deposition times of 3 and 5 min, for each voltage. Figure 1 shows the scheme for cathodic deposition.
2. The FTO and the ZnO films were retrieved from the suspension and then calcined with a thermal treatment at 450 °C for 30 min.

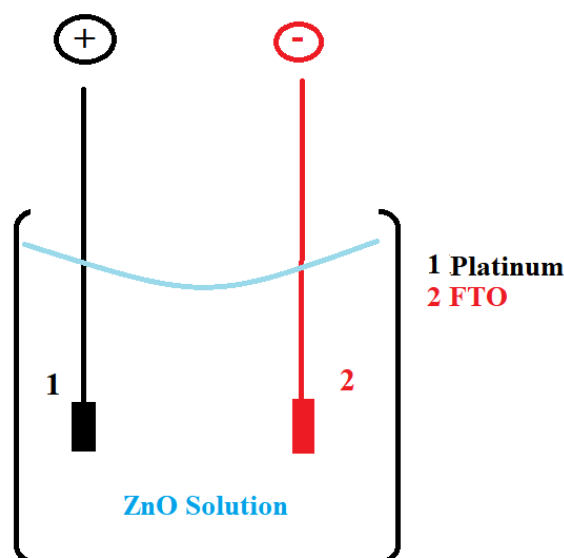


Figure 1. Scheme of the electrophoresis cell.

The assembly of the cells followed the following steps:

1. The FTO was immersed in N719 ruthenium-based dye for 24 h.
2. The FTO/dye was coupled with the platinum.
3. AN-50 electrolyte was injected between the sandwiched electrodes.
4. The cells were tested under light simulation following procedures outlined by Nunes. V.F et al. [34].

In the EPD process, a uniform film was obtained through the electrophoresis of the charged ZnO particles in the suspension on the FTO substrate under the electric field applied by the ddp source [35].

2.2. Characterization of the Films

The structural characterization was performed using X-ray diffraction, using an Aeris-Panalytical diffractometer. Spectrophotometer tests in the UV range (between 200 and 700 nm) were performed at room temperature using a Shimadzu UV-2600 (Shimadzu, Kyoto City, Japan) equipped with ISR-2600Plus. The Kubelka-Munk method [36] was used to transform the relative diffuse reflectivity into absorbance data.

Solar tests under 100 mW/cm² LED illumination and impedance tests were conducted using an AUTOLAB (PGSTAT302N, Metrohm, Herisau, Switzerland). The FRA (Frequency response analyzer) (AMETEK, Berwyn, PA, USA) software, FRA v 35, was used for electrochemical impedance spectroscopy (EIS) experiments. The cells were kept illuminated throughout the tests.

3. Results and Discussion

3.1. XRD Analysis

The films deposited by electrophoresis were subjected to XRD analysis over a range of 20 to 80° to obtain information about the peaks, their positions, and intensities (Figure 2). The observed peaks were (100), (002), (101), (102), (110), (103), and (200). The predominant peak among all six deposited films was (101), indicating the preferred growth orientation of the structure. These peaks are consistent with the wurtzite structure of zinc oxide, as reported in [19]. The crystallite sizes for the films were calculated using the Scherrer equation:

$$D = k\lambda / \beta \cos \theta, \quad (1)$$

where D is the crystallite size, k is the Scherrer constant (0.9), λ is the wavelength of 0.15406 nm, β is the FWHM (rad) (full width at half maximum), and θ is the Bragg angle position.

The calculated crystallite sizes were 83.09 nm, 79.89 nm and 76.76 nm for the films deposited for 3 min at 60 V, 70 V and 80 V, respectively and 78.69 nm, 86.72 nm, and 95.2 nm for the films deposited for 3 min at 60 V, 70 V and 80 V, respectively. At 3 min of electrophoresis deposition time, an increase in the applied voltage led to an increase in the intensity of the peaks. Conversely, for a deposition time of 5 min, the intensity of the peaks decreased with increasing the applied voltage from 60 V to 70 V. The narrow widths of the peaks indicated good crystallinity quality for the deposited films.

3.2. UV Analysis

The absorption spectra of the ZnO thin films (Figure 3a,b) reveal peaks within the 300 to 400 nm range, with additional peaks emerging for longer deposition times, specifically at 5 min. All films consistently demonstrated reflectance values ranging from 60% to 90%, as illustrated in Figure 3c,d, indicating their suitability for application in optical devices. Furthermore, an increase in deposition time was observed to positively impact overall reflectance, signifying an enhancement in optical quality.

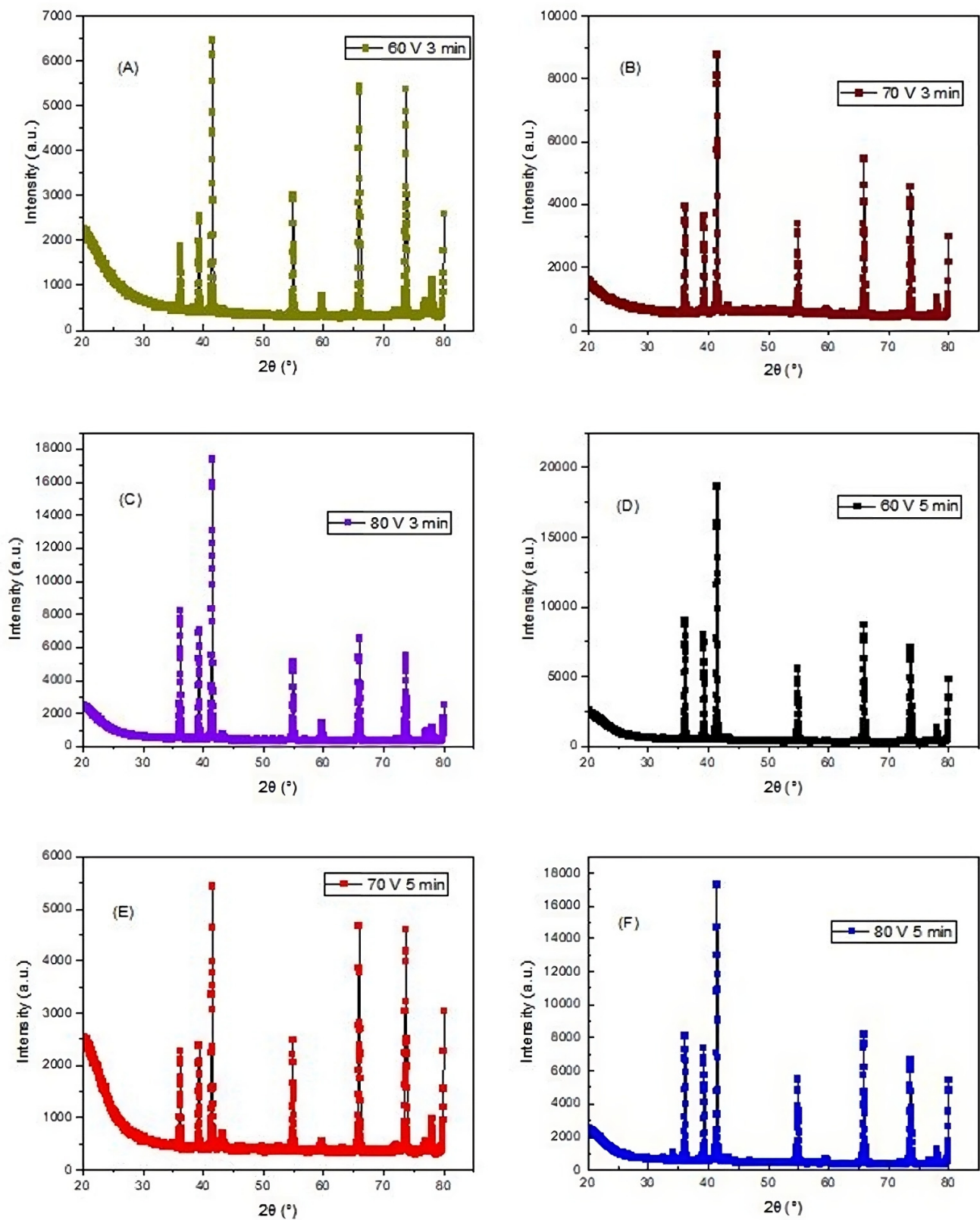


Figure 2. XRD analysis for the deposited films at (A) 60 V and 3 min; (B) 70 V and 3 min; (C) 80 V and 3 min; (D) 60 V and 5 min; (E) 70 V and 5 min; and (F) 80 V and 5 min.

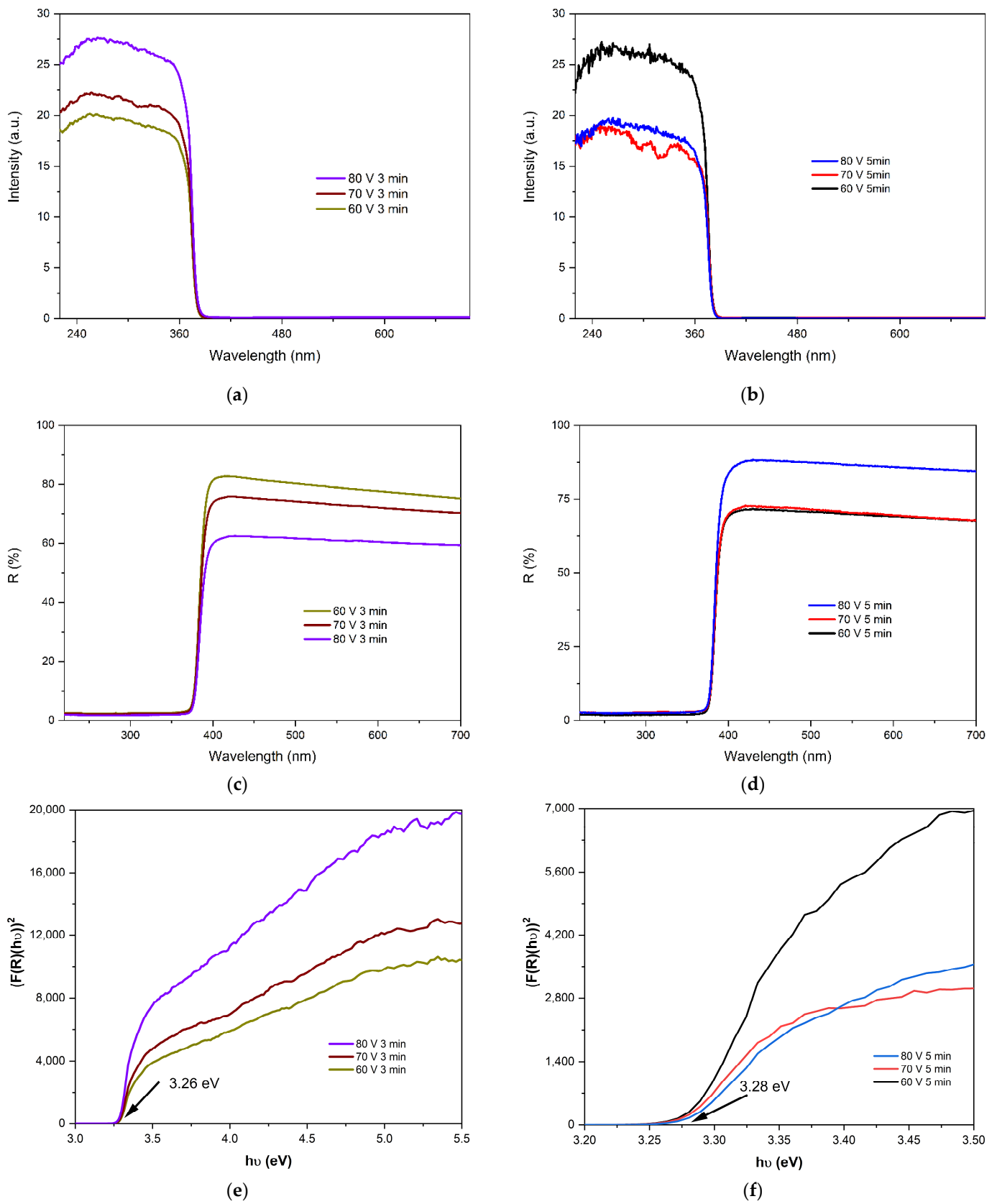


Figure 3. (a) Absorbance at 3 min; (b) absorbance at 5 min; (c) reflectance at 3 min; (d) reflectance at 5 min; (e) Kubelka–Munk at 3 min; (f) Kubelka–Munk at 5 min deposition time.

UV analysis of the Kubelka–Munk plots (Figure 3e,f) resulted in estimated band gap values of 3.26 eV at 3 min and 3.28 eV at 5 min for the electrophoretic deposition time. This suggests that varying the electrophoresis deposition time did not significantly affect the band gap energy of the films. Equations (2) and (3) describe the Kubelka–Munk function (F(R)) [7]:

$$[F(R) \text{ } hv] = A (hv - E_g)^n, \quad (2)$$

In the context of UV–Vis analyses, A represents the absorbance values acquired. Here, hv denotes the photon energy, E_g signifies the band gap values, and n assumes a value of 2 specifically in the case of direct band gap values for ZnO.

$$F(R) = (1 - R)^2 / 2R, \quad (3)$$

where R is the material's reflectance value analyzed by the spectrophotometer.

The Tauc plot, which is a graphical representation, was used to estimate the thicknesses of the thin films represented in Table 1 based on their optical absorption spectra. The Tauc plot involves plotting the square of the absorption coefficient (α) (Equation (4)) against the photon energy (hv). The intercept of the extrapolated linear portion of the curve with the energy axis provides an estimate of the band gap energy (E_g), which, in turn, can be related to the thickness of the film.

$$\alpha = A/d = -\text{Ln}(1/T)/d, \quad (4)$$

Table 1. Thickness of the ZnO films.

ZnO Film	Thickness (μm)
60 V_3 min	2.02
70 V_3 min	2.05
80 V_3 min	2.08
60 V_5 min	2.1
70 V_5 min	2.0
80 V_5 min	2.02

In Equation (3), the absorption A can be estimated by the Kubelka–Munk relation, $F(R)$, and T is the transmittance value, which can be calculated by the absorbance values in Figure 3a,b. The thicknesses of the electrodeposited films were consistently around 2 μm , indicating that the increase in deposition time was generally not significant. However, for the films deposited at a voltage of 60 V, a slightly higher difference was observed for films deposited at 3 min (2.02 μm) and 5 min (2.1 μm), resulting in an increase of 4% in thickness. The uniform thickness values align with the consistent band gap values for the films. Lyalin et al. [23] also observed that in electrophoretic deposition (EPD), changes in thickness mainly occur within the first minute, while from 3 to 6 min, the deposition rate remains relatively constant. This phenomenon can be attributed to the increase in resistance; as the thickness grows, the resistance on the FTO also increases, leading to a decrease in the deposition rate [37].

Figure 4a,b show the transmittance values for the films deposited at 3 and 5 min, respectively. All the EPD films exhibited high transmittance in the visible range of the spectrum, ranging from 75 to 95%, and very low transmittance values in the ultraviolet spectra, where photon absorption and the transition from the valence to conduction band occur. The films deposited at 5 min exhibited superior transmittance quality, particularly evident at 80 V, where it increased from 75% for the films deposited at 3 min to 95% for the films deposited at 5 min, representing a 20% improvement with a longer deposition time. However, at 60 V, the transmittance decreased for the films with an increased deposition time, suggesting increased light absorbance.

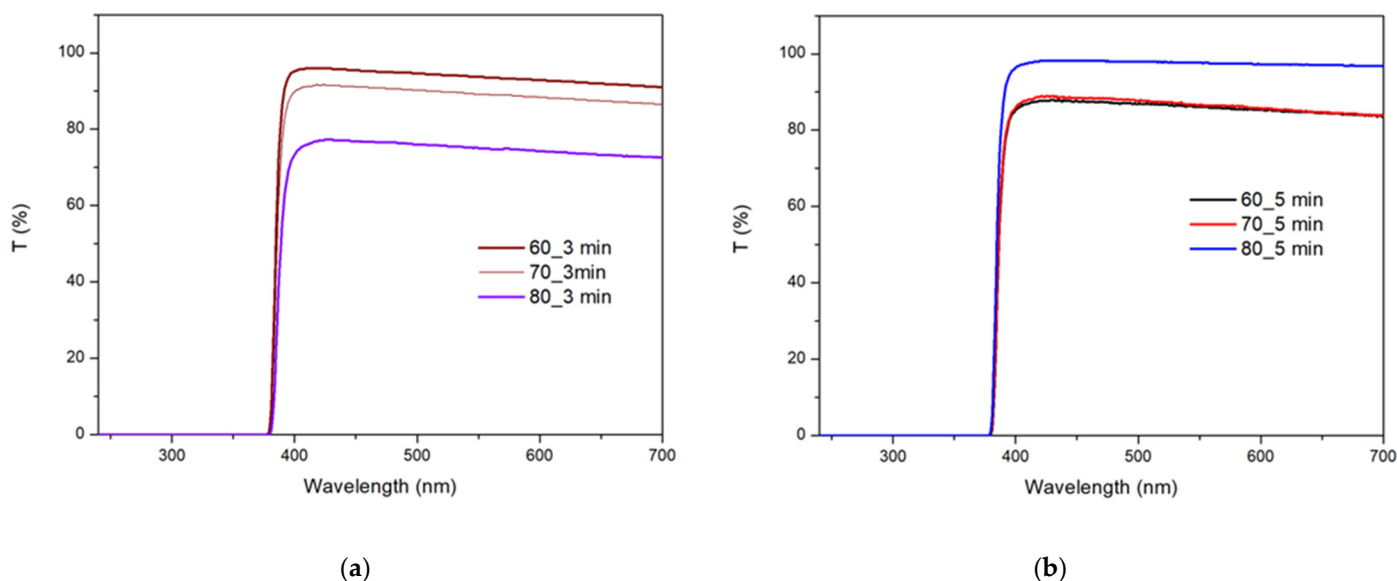


Figure 4. Transmittance spectra for the films electrodeposited at (a) 3 min and (b) 5 min.

3.3. Electrochemical Impedance Spectroscopy (EIS)

Electrochemical impedance spectroscopy was employed to examine the interfacial charge behavior of the dye cells, illustrated through Nyquist and Bode plots in Figure 5. In Figure 5c, semicircles are evident in the high-frequency region, indicating resistance to charge transport at the interface between the electrolyte (3I-/I-3) and platinum, thereby impacting the overall cell resistance. Notably, cells with thin films deposited for 3 min (Figure 4a) exhibit higher resistance [38].

From the Bode plots (Figure 5b,d), the electron lifetimes (τ) were calculated and are presented in Table 2. The τ (ms) values were determined using the equation $\tau = 1/(2\pi f_p)$, where f_p represents the highest frequency at the ZnO/electrolyte interface [39]. It is noteworthy that all calculated electron lifetimes for the cells were relatively low, thereby influencing the incident photocurrent efficiency (IPCE) within the cells.

Table 2. Electron lifetime of the films.

ZnO Film	Electron Lifetime (ms)
60 V_3 min	2.1
70 V_3 min	5.4
80 V_3 min	2.6
60 V_5 min	1.5
70 V_5 min	2.3
80 V_5 min	5.1

3.4. Photovoltaic Results

The current density results are close to those reported in [38]. A comparison of the outcomes, presented in Figure 6a,b, reveals a notably enhanced photovoltaic short-circuit current density (J_{sc}) for the thin films deposited for 5 min. This suggests that a 24 h dye adsorption time combined with a 5 min deposition time yielded a thicker film with effective dye adsorption. Conversely, the 3 min deposition resulted in the formation of dye/ZnO aggregates, diminishing both the short-circuit current density and the Incident Photocurrent Efficiency (IPCE). This phenomenon, where dye/ZnO particles obstruct electron flow, is a common observation in dye solar cells utilizing zinc oxide. The IPCE is a function of the light conversion efficiency, electrode injection, and counter electrode injection. The increase in deposition time led to an enhancement in the current density of the cells, suggesting that a longer deposition time improved the crystallite quality and,

consequently, the electron path, thereby reducing hole–electron recombination. The voltage increase was more significant at 3 min of deposition, where the increase from 60 to 70 V also raised the photocurrent conversion from 1.28 to 2.57. At 5 min, the photovoltaic values for 60 and 70 V were close. However, a reduction was observed for 80 V due to a lower Fill Factor (FF), indicating reduced stability.

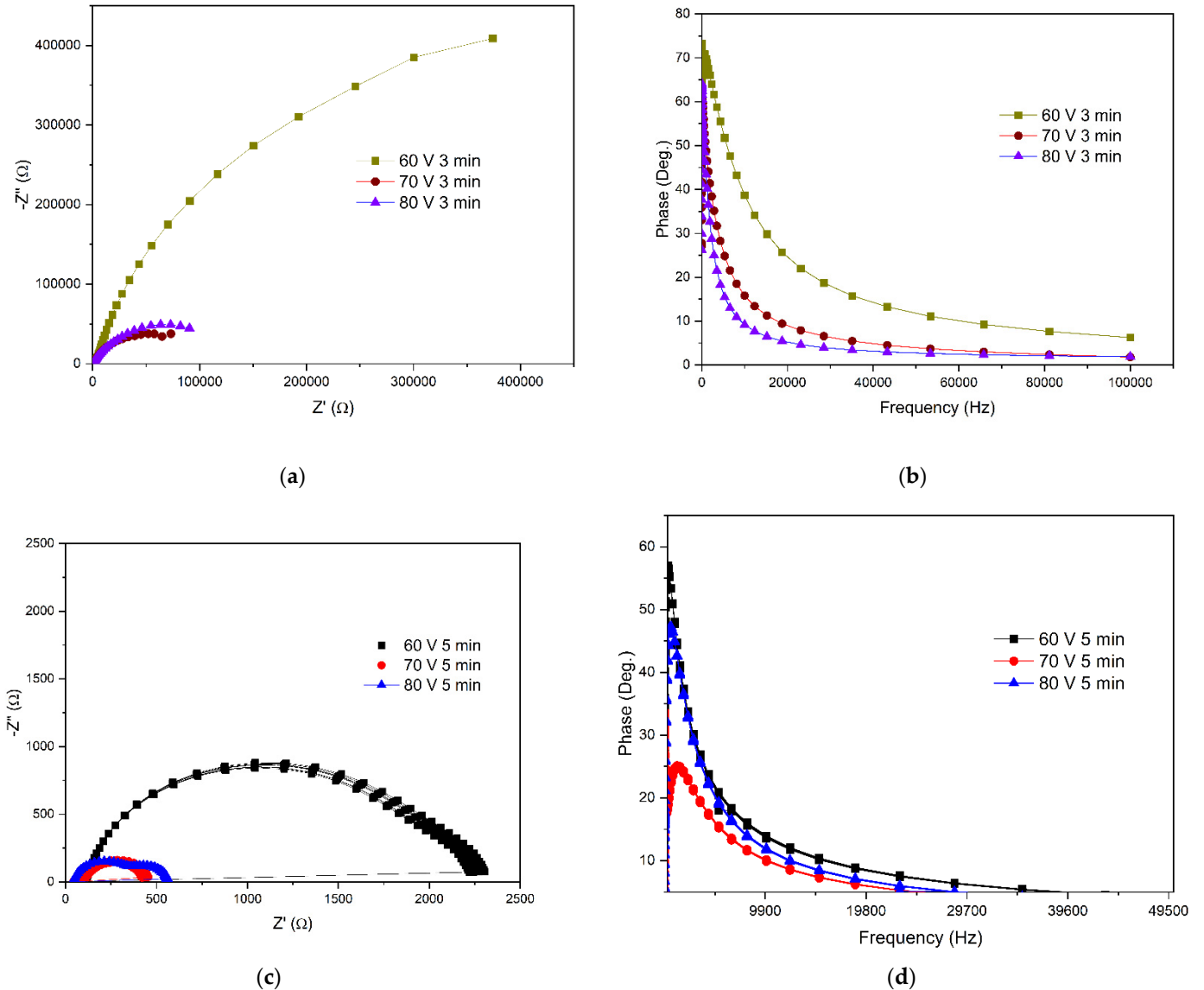


Figure 5. (a) Nyquist plot for the 3 min deposition time; (b) Bode plot for the 3 min; (c) Nyquist plot for the 5 min; and (d) Bode plot for the 5 min deposition time.

The open-circuit voltage (V_{oc}) of all cells remained consistent due to the identical assembly of cells with the same electrolytes, dyes, and counter electrodes. The thin film deposited at 70 V and 5 min exhibited the highest fill factor (FF) of 0.51, indicating improved cell stability. This particular cell demonstrated the highest efficiency among the assembled DSSCs, attributed to its FF of 0.51 and short current density of 1.94 mA/cm^2 (Table 3). These values closely align with those found in other studies where ZnO was employed in DSSCs [35,40].

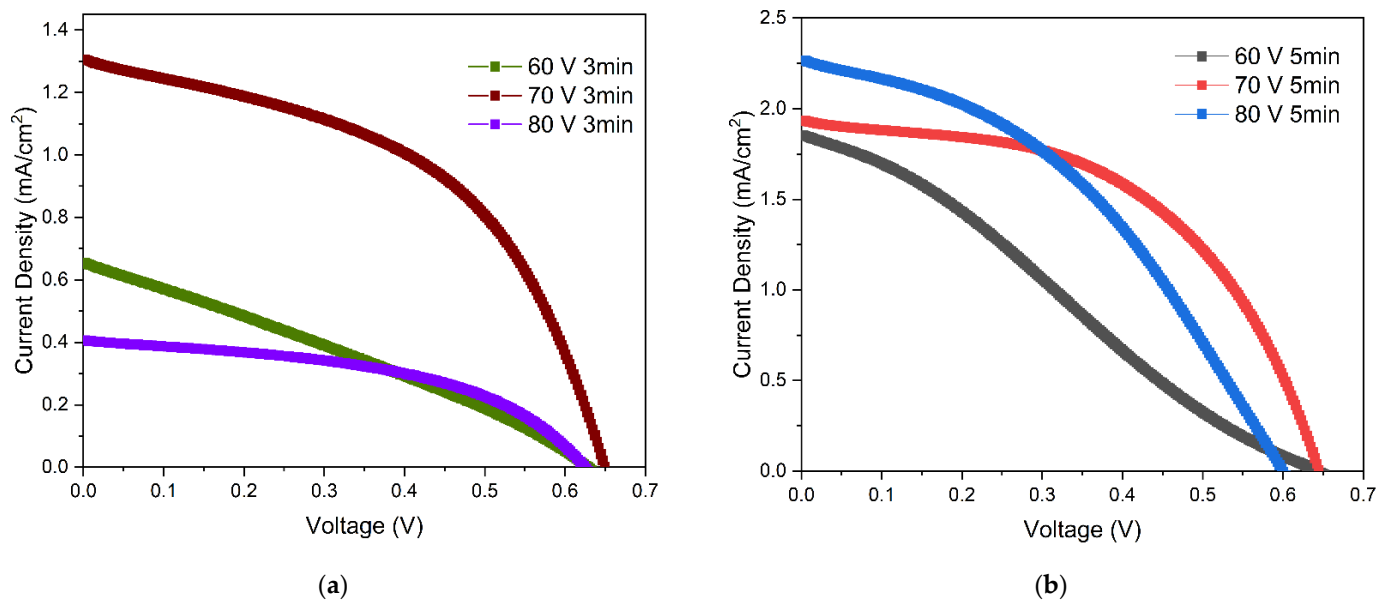


Figure 6. J-V data of the EPD films at (a) 3 min (b) 5 min deposition time.

Table 3. Parameters of the photovoltaic tests.

Deposition Time	3 min			5 min		
	60	70	80	60	70	80
Jsc (mA/cm ²)	0.65	1.30	0.40	1.80	1.94	2.27
FF	0.29	0.48	0.47	0.19	0.51	0.40
Efficiency (%)	0.12	0.40	0.12	0.20	0.64	0.55
Voc (V)	0.64	0.66	0.63	0.66	0.65	0.61
IPCE (%)	1.28	2.57	0.80	3.52	3.80	4.48
Rsh (Ω/cm ²)	1222	194.7	6333.3	1360	1400	750
Rs (Ω/cm ²)	750	168	476.2	250	108.4	163.6

As the applied voltage increases, the mass variation of deposited ZnO decreases, particularly with more deposition time. Hasanpoor et al. [41] observed that above 40 V, the mass of zinc oxide deposited on the FTO electrode stabilizes after 200 s. This occurs because the higher voltage results in a greater mass density, causing the gravitational force to become greater than the electrical field. Additionally, the deposition of more layers increases the resistance to the formation of a film on the electrode surface. This affects the thickness of the films, typically around micrometers, as observed above, and also increases series resistance, thereby reducing the overall efficiency of the assembled cells. For cells with lower series resistance (R_s), the short-circuit current density (J_{sc}) increased, as shown in Table 3. Conversely, for cells with higher R_s , the J_{sc} declined. The cells with the highest IPCE values, obtained at 80V for 5min, exhibited a shunt resistance (R_{sh}) of 750 Ω/cm² and a series resistance (R_s) of 163.6 Ω/cm².

The IPCE was calculated according to equation 5 [42]:

$$\text{IPCE (\%)} = (hc J_{sc}) / (\lambda \Phi), \quad (5)$$

where $hc = 1240$ (eV nm), λ is the wavelength (nm), Φ is the intensity (mW/cm²), and J_{sc} is the short circuit photocurrent density (mA/cm²).

The fill factor (FF) was calculated according to Equation (6) and efficiency η according to Equation (7) [43]:

$$FF = (J_m V_m) / (J_{sc} V_{oc}), \quad (6)$$

$$\eta (\%) = ((FF J_{sc} V_{oc}) / P_{in}) \times 100, \quad (7)$$

where J_m (mA/cm²) and V_m (V) are the maximum current and voltage, respectively. J_{sc} is the short current (mA/cm²), V_{oc} (V) is the open circuit voltage and P_{in} is the input power of 100 mW/cm². The series resistance (R_s) and shunt resistance (R_{sh}) were calculated according to [44].

Photovoltaic values for the ZnO films are comparable to those obtained by Shakir. S. et al. [30], who used a multistep EPD method for TiO₂, achieving an efficiency of 1.28%, a fill Factor (FF) of 0.67, a short current density (J_{sc}) of 2.69 mA/cm², and an open-circuit voltage (V_{oc}) of 0.67 V. Vasanth. A. et al. [32] used EPD of graphene on TiO₂, achieving a 2% efficiency after 20 min of deposition and a 6% efficiency for 5 min of EPD. However, the photovoltaic parameters decreased with a longer deposition time. Giannouli et al. [42] achieved an IPCE of 0.6% using ZnO nanowires in DSSCs. Lai et al. [45] obtained efficiencies ranging from 0.4 to 0.74% by employing ZnO nanorods in DSSCs, indicating that the formation of complexes of Zn²⁺/dyes contributed to a reduction in the overall electron injection efficiency.

4. Conclusions

The electrophoretic deposition method successfully generated thin zinc oxide films on conductive glass substrates using three different voltage levels, 60 V, 70 V, and 80 V, with deposition times of both 3 and 5 min.

Spectrophotometry analysis revealed the production of thin films with favorable reflectance in the visible range of the spectra, ranging between 60% and 90%, and band gap values at approximately 3.28 eV, slightly lower than the typical 3.3 eV for ZnO. These films functioned as photoanodes for dye-sensitized solar cells.

The results showcased enhanced photovoltaic performance for the photoanodes deposited through electrophoretic deposition for 5 min at 70 V and 80 V, resulting in Incident Photocurrent Efficiency (IP-CE) values of 3.8% and 4.48%, respectively. This method demonstrated efficiency in depositing photoconductive material.

EPD is not a widely used method applied in DSSCs due to challenges associated with achieving a homogeneous film without cracks, and this is essential for improving the parameters of the solar cell. To address these issues, various tests can be conducted, such as reducing the deposition time or minimizing the contact time between the film and the dye. Additionally, the combination of ZnO with other elements that increase the electron injection into the cell can lead to further improvements. This work intended to amplify the use of EPD in renewable energy beyond the typical focus on the bio applications often found in the literature.

Author Contributions: Conceptualization, M.P.F.G. and F.N.A.F.; methodology, A.F.L.A., F.N.A.F. and V.F.N.; software, V.F.N. and I.H.; validation, M.P.F.G., F.N.A.F. and A.F.L.A.; formal analysis, V.F.N. and A.F.L.A.; investigation, V.F.N.; resources, M.P.F.G. and F.N.A.F.; data curation, V.F.N. and I.H.; writing—original draft preparation, V.F.N.; writing—review and editing, I.H., F.N.A.F. and M.P.F.G.; visualization, I.H.; supervision, F.N.A.F.; project administration, F.N.A.F.; funding acquisition, F.N.A.F. and M.P.F.G. All authors have read and agreed to the published version of the manuscript.

Funding: This research was funded by FEDER funds through the COMPETE 2020 Program and National Funds through FCT—Portuguese Foundation for Science and Technology under the projects LISBOA-01-0247-FEDER-039985/POCI-01-0247-FEDER-039985, LA/P/0037/2020, UIDP/50025/2020, and UIDB/50025/2020 of the Associate Laboratory Institute of Nanostructures, Nanomodelling and Nanofabrication—i3N.

Institutional Review Board Statement: Not applicable.

Informed Consent Statement: Not applicable.

Data Availability Statement: The data presented in this study are available on request from the corresponding author.

Acknowledgments: The authors would like to acknowledge the Brazilian fund Capes, Coordenação de Aperfeiçoamento de Pessoal de Nível Superior, and the Laboratory of Thin Films and Renewable Energy LAFFER.

Conflicts of Interest: The authors declare no conflict of interest.

References

1. Ikpesu, J.E.; Iyuke, S.E.; Daramola, M.; Okewale, A.O. Synthesis of Improved Dye-Sensitized Solar Cell for Renewable Energy Power Generation. *Sol. Energy* **2020**, *206*, 918–934. [[CrossRef](#)]
2. Fernandes, P.A.; Sartori, A.F.; Salomé, P.M.P.; Malaquias, J.; Da Cunha, A.F.; Graça, M.P.F.; González, J.C. Admittance Spectroscopy of $\text{Cu}_2\text{ZnSnS}_4$ Based Thin Film Solar Cells. *Appl. Phys. Lett.* **2012**, *100*, 233504. [[CrossRef](#)]
3. Zhang, Q.; Cao, G. Nanostructured Photoelectrodes for Dye-Sensitized Solar Cells. *Nano Today* **2011**, *6*, 91–109. [[CrossRef](#)]
4. Bisquert, J. Dilemmas of Dye-Sensitized Solar Cells. *ChemPhysChem* **2011**, *12*, 1633–1636. [[CrossRef](#)]
5. Pugazhendhi, K.; Praveen, B.; Sharmila, D.J.; Mary, J.S.S.; Kumar, P.N.; Bharathilenin, V.; Shyla, J.M. Plasmonic $\text{TiO}_2/\text{Al@ZnO}$ Nanocomposite-Based Novel Dye-Sensitized Solar Cell with 11.4% Power Conversion Efficiency. *Sol. Energy* **2021**, *215*, 443–450. [[CrossRef](#)]
6. Chou, T.P.; Zhang, Q.; Russo, B.; Cao, G. Enhanced Light-Conversion Efficiency of Titanium-Dioxide Dye-Sensitized Solar Cells with the Addition of Indium-Tin-Oxide and Fluorine-Tin-Oxide Nanoparticles in Electrode Films. *J. Nanophotonics* **2008**, *2*, 023511. [[CrossRef](#)]
7. Javed, A.H.; Shahzad, N.; Khan, M.A.; Ayub, M.; Iqbal, N.; Hassan, M.; Hussain, N.; Rameel, M.I.; Shahzad, M.I. Effect of ZnO Nanostructures on the Performance of Dye Sensitized Solar Cells. *Sol. Energy* **2021**, *230*, 492–500. [[CrossRef](#)]
8. Lu, L.; Li, R.; Fan, K.; Peng, T. Effects of Annealing Conditions on the Photoelectrochemical Properties of Dye-Sensitized Solar Cells Made with ZnO Nanoparticles. *Sol. Energy* **2010**, *84*, 844–853. [[CrossRef](#)]
9. Raha, S.; Ahmaruzzaman, M. ZnO Nanostructured Materials and Their Potential Applications: Progress, Challenges and Perspectives. *Nanoscale Adv.* **2022**, *4*, 1868–1925. [[CrossRef](#)] [[PubMed](#)]
10. Yoshihara, T.; Katoh, R.; Furube, A.; Murai, M.; Tamaki, Y.; Hara, K.; Murata, S.; Arakawa, H.; Tachiya, M. Quantitative Estimation of the Efficiency of Electron Injection from Excited Sensitizer Dye into Nanocrystalline ZnO Film. *J. Phys. Chem. B* **2004**, *108*, 2643–2647. [[CrossRef](#)]
11. Ye, N.; Qi, J.; Qi, Z.; Zhang, X.; Yang, Y.; Liu, J.; Zhang, Y. Improvement of the Performance of Dye-Sensitized Solar Cells Using Sn-Doped ZnO Nanoparticles. *J. Power Sources* **2010**, *195*, 5806–5809. [[CrossRef](#)]
12. Suresh, S.; Pandikumar, A.; Murugesan, S.; Ramaraj, R.; Raj, S.P. Photovoltaic Performance of Solid-State Solar Cells Based on ZnO Nanosheets Sensitized with Low-Cost Metal-Free Organic Dye. *Sol. Energy* **2011**, *85*, 1787–1793. [[CrossRef](#)]
13. Wu, P.; Pike, J.; Zhang, F.; Chan, S. Low-Temperature Synthesis of Zinc Oxide Nanoparticles. *Int. J. Appl. Ceram. Technol.* **2006**, *3*, 272–278. [[CrossRef](#)]
14. Zhang, Q.; Dandeneau, C.S.; Zhou, X.; Cao, G. ZnO Nanostructures for Dye-Sensitized Solar Cells. *Adv. Mater.* **2009**, *21*, 4087–4108. [[CrossRef](#)]
15. Wojtyła, S.; Baran, T. Copper Zinc Oxide Heterostructure Nanoflowers for Hydrogen Evolution. *Int. J. Hydrogen Energy* **2019**, *44*, 27343–27353. [[CrossRef](#)]
16. Javed, M.; Qamar, M.A.; Shahid, S.; Alsaab, H.O.; Asif, S. Highly Efficient Visible Light Active Cu–ZnO/S-g- C_3N_4 Nanocomposites for Efficient Photocatalytic Degradation of Organic Pollutants. *RSC Adv.* **2021**, *11*, 37254–37267. [[CrossRef](#)]
17. Di Mauro, A.; Fragalà, M.E.; Privitera, V.; Impellizzeri, G. ZnO for Application in Photocatalysis: From Thin Films to Nanostructures. *Mater. Sci. Semicond. Process.* **2017**, *69*, 44–51. [[CrossRef](#)]
18. Bhogaita, M.; Devaprakasam, D. Hybrid Photoanode of TiO_2 -ZnO Synthesized by Co-Precipitation Route for Dye-Sensitized Solar Cell Using *Phyllanthus Reticulatas* Pigment Sensitizer. *Sol. Energy* **2021**, *214*, 517–530. [[CrossRef](#)]
19. Nunes, V.F.; Teixeira, E.S.; Maia Júnior, P.H.F.; Almeida, A.F.L.; Freire, F.N.A. Study of Electrophoretic Deposition of ZnO Photoanodes on Fluorine-Doped Tin Oxide (FTO) Glass for Dye-Sensitized Solar Cells (DSSCs). *Cerâmica* **2022**, *68*, 120–125. [[CrossRef](#)]
20. Selvinsimpson, S.; Gnanamozi, P.; Pandiyan, V.; Govindasamy, M.; Habila, M.A.; AlMasoud, N.; Chen, Y. Synergetic Effect of Sn Doped ZnO Nanoparticles Synthesized via Ultrasonication Technique and Its Photocatalytic and Antibacterial Activity. *Environ. Res.* **2021**, *197*, 111115. [[CrossRef](#)]
21. Tarwal, N.L.; Patil, V.L.; Rani, J.R.; Gurav, K.V.; Shaikh, J.S.; Khandekar, M.S.; Harale, N.S.; Patil, P.S.; Jang, J.H. Plasmonic DSSC Performance of Spray Deposited Ag-ZnO and Au-ZnO Films. *Chin. J. Phys.* **2021**, *73*, 581–588. [[CrossRef](#)]
22. Schneider, M.; Weiser, M.; Ferl, S.; Krasmann, C.; Potthoff, A.; Voigt, K.; Malcher, P. Facile Deposition of Multiwalled Carbon Nanotubes via Electrophoretic Deposition in an Environmentally Friendly Suspension. *Surf. Coat. Technol.* **2021**, *406*, 126741. [[CrossRef](#)]
23. Lyalin, E.; Il'ina, E.; Kalinina, E.; Antonov, B.; Pankratov, A.; Pereverzev, D. Electrophoretic Deposition and Characterization of Thin-Film Membranes $\text{Li}_7\text{La}_3\text{Zr}_2\text{O}_{12}$. *Membranes* **2023**, *13*, 468. [[CrossRef](#)] [[PubMed](#)]

24. Pröller, S.; Filonik, O.; Eller, F.; Mansi, S.; Zhu, C.; Schaible, E.; Hexemer, A.; Müller-Buschbaum, P.; Herzig, E.M. Electrophoresis Assisted Printing: A Method To Control the Morphology in Organic Thin Films. *ACS Appl. Mater. Interfaces* **2020**, *12*, 5219–5225. [[CrossRef](#)] [[PubMed](#)]
25. Das, D.; Bagchi, B.; Basu, R.N. Nanostructured Zirconia Thin Film Fabricated by Electrophoretic Deposition Technique. *J. Alloys Compd.* **2017**, *693*, 1220–1230. [[CrossRef](#)]
26. Liu, Y.; Ren, L.; Zhang, Z.; Qi, X.; Li, H.; Zhong, J. 3D Binder-Free MoSe₂ Nanosheets/Carbon Cloth Electrodes for Efficient and Stable Hydrogen Evolution Prepared by Simple Electrophoresis Deposition Strategy. *Sci. Rep.* **2016**, *6*, 22516. [[CrossRef](#)]
27. Zargazi, M.; Entezari, M.H. Anodic Electrophoretic Deposition of Bi₂WO₆ Thin Film: High Photocatalytic Activity for Degradation of a Binary Mixture. *Appl. Catal. B Environ.* **2019**, *242*, 507–517. [[CrossRef](#)]
28. Pikalova, E.; Osinkin, D.; Kalinina, E. Direct Electrophoretic Deposition and Characterization of Thin-Film Membranes Based on Doped BaCeO₃ and CeO₂ for Anode-Supported Solid Oxide Fuel Cells. *Membranes* **2022**, *12*, 682. [[CrossRef](#)] [[PubMed](#)]
29. Hassam, C.L.; Sciortino, F.; Nguyen, N.T.K.; Srinivasan, B.; Ariga, K.; Gascoin, F.; Grasset, F.; Mori, T.; Uchikoshi, T.; Thimont, Y.; et al. Robust, Transparent Hybrid Thin Films of Phase-Change Material Sb₂S₃ Prepared by Electrophoretic Deposition. *ACS Appl. Energy Mater.* **2021**, *4*, 9891–9901. [[CrossRef](#)]
30. Shakir, S.; Abd-ur-Rehman, H.M.; Zahid, R.; Iwamoto, M.; Periasamy, V. Multistep Electrophoretic Deposition of TiO₂ Film and Its Surface Modification for Dye Sensitized Solar Cells. *J. Alloys Compd.* **2020**, *837*, 155579. [[CrossRef](#)]
31. Yaacob, K.A.; Keoh, D.L.; Kyaw, H.M.A.; Ishak, M.N. CdSe-TiO₂ Nanocomposites Film Deposited by Electrophoretic Co-Deposition towards Quantum Dots Sensitized Solar Cells. *Mater. Today Proc.* **2022**, *66*, 3144–3149. [[CrossRef](#)]
32. Vasanth, A.; Powar, N.S.; Krishnan, D.; Nair, S.V.; Shanmugam, M. Electrophoretic Graphene Oxide Surface Passivation on Titanium Dioxide for Dye Sensitized Solar Cell Application. *J. Sci. Adv. Mater. Devices* **2020**, *5*, 316–321. [[CrossRef](#)]
33. Aghili, F.; Hoomehr, B.; Saidi, R.; Raeissi, K. Synthesis and Electrophoretic Deposition of Zinc Oxide and Zinc Oxide-Bioactive Glass Composite Nanoparticles on AZ₃₁ Mg Alloy for Biomedical Applications. *Ceram. Int.* **2022**, *48*, 34013–34024. [[CrossRef](#)]
34. Nunes, V.F.; Lima, F.M.; Teixeira, E.S.; Maia Júnior, P.H.F.; Almeida, A.F.L.; Freire, F.N.A. Synthesis of TiO₂/ZnO Photoanodes on FTO Conductive Glass for Photovoltaic Applications. *Cerâmica* **2023**, *69*, 79–86. [[CrossRef](#)]
35. Das, P.P.; Roy, A.; Devi, P.S.; Lee, Y. Solution Processed Al-Doped ZnO and Its Performance in Dye Sensitized Solar Cells. *Curr. Appl. Phys.* **2021**, *30*, 69–76. [[CrossRef](#)]
36. Munk, K. The Kubelka-Munk Theory of Reflectance, *Zeit. Fur Tekn. Phys.* **1931**, *12*, 593.
37. Wang, Y.; Leu, I.; Hon, M. Kinetics of Electrophoretic Deposition for Nanocrystalline Zinc Oxide Coatings. *J. Am. Ceram. Soc.* **2004**, *87*, 84–88. [[CrossRef](#)]
38. Ranamagar, B.; Abiye, I.; Karki, H.; Lan, Y.; Abebe, F. Performance of Rhodamine-Sensitized Solar Cells Fabricated with Silver Nanoparticles. *Adv. Nanoparticles* **2023**, *12*, 68–79. [[CrossRef](#)]
39. Chen, X.; Tang, Y.; Liu, W. Efficient Dye-Sensitized Solar Cells Based on Nanoflower-like ZnO Photoelectrode. *Molecules* **2017**, *22*, 1284. [[CrossRef](#)] [[PubMed](#)]
40. Esgin, H.; Caglar, Y.; Caglar, M. Photovoltaic Performance and Physical Characterization of Cu Doped ZnO Nanopowders as Photoanode for DSSC. *J. Alloys Compd.* **2022**, *890*, 161848. [[CrossRef](#)]
41. Hasanpoor, M.; Aliofkhaezrai, M.; Delavari, H.H. In-Situ Study of Mass and Current Density for Electrophoretic Deposition of Zinc Oxide Nanoparticles. *Ceram. Int.* **2016**, *42*, 6906–6913. [[CrossRef](#)]
42. Giannouli, M.; Govatsi, K.; Syrokostas, G.; Yannopoulos, S.N.; Leftheriotis, G. Factors Affecting the Power Conversion Efficiency in ZnO DSSCs: Nanowire vs. Nanoparticles. *Materials* **2018**, *11*, 411. [[CrossRef](#)]
43. Siregar, N.; Motlan, U.; Panggabean, J.H.; Sirait, M.; Rajagukguk, J.; Gultom, N.S.; Sabir, F.K. Fabrication of Dye-Sensitized Solar Cells (DSSC) Using Mg-Doped ZnO as Photoanode and Extract of Rose Myrtle (*Rhodomyrtus tomentosa*) as Natural Dye. *Int. J. Photoenergy* **2021**, *2021*, e4033692. [[CrossRef](#)]
44. Benghanem, M.S.; Alamri, S.N. Modeling of Photovoltaic Module and Experimental Determination of Serial Resistance. *J. Taibah Univ. Sci.* **2009**, *2*, 94–105. [[CrossRef](#)]
45. Lai, F.-I.; Yang, J.-F.; Hsu, Y.-C.; Lin, K.-J.; Kuo, S.-Y. Enhancing DSSC Performance through Manipulation of the Size of ZnO Nanorods. *ACS Omega* **2023**, *8*, 40206–40211. [[CrossRef](#)] [[PubMed](#)]

Disclaimer/Publisher’s Note: The statements, opinions and data contained in all publications are solely those of the individual author(s) and contributor(s) and not of MDPI and/or the editor(s). MDPI and/or the editor(s) disclaim responsibility for any injury to people or property resulting from any ideas, methods, instructions or products referred to in the content.